Catalytic Oxidation of Hydrogen—Intrapellet Heat and Mass Transfer

J. A. MAYMO and J. M. SMITH

University of California, Davis, California

Rates of oxidation of hydrogen were measured by using platinum–alumina catalyst particles and 1.86-cm. pellets. For high-reaction rates, temperature differences between center and surface of the pellets were more than 300°C. Under these conditions large variations in temperature with position on the pellet surface were observed. The pellet reactor was of the recirculation, stirred-tank type with injection nozzles. Local heat transfer coefficients between pellet and gas varied twofold with location on the surface. The data showed that intrapellet heat and mass transfer resistances were both important, while between pellet and gas only the heat transfer resistance was significant.

The effective thermal conductivity of the pellet was measured independently. By using this and the experimental temperature measurements, a new method is devised to establish the effective diffusivity under reaction conditions.

Effectiveness factors were predicted from k_e and D_e and the rate data for the particles. The results were about 7% greater than the experimental effectiveness factor.

The necessity of mass and energy transfer for steady state performance of porous catalyst pellets requires intrapellet concentration and temperature gradients. The effect of these gradients on the overall kinetics has been accounted for traditionally by the use of an effectiveness factor. The combined influence of both transport processes has been described analytically in several investigations (*1* to *3*) and the whole subject has been reviewed by Satterfield and Sherwood (*4*). Such studies predict large temperature differences within catalyst pellets for highly exothermic or endothermic reactions on solids of low thermal conductivity. Most porous catalysts do have surprisingly small thermal conductivities (*5, 6*).

Besides modifying the effectiveness factor, temperature gradients may cause a favorable shift in equilibrium constants. Side reactions which were impossible at pellet surface temperature may have appreciable equilibrium conversions at conditions within the pellet. In extreme cases chemical and mechanical changes in the catalyst itself may occur. Despite the recognition theoretically of large temperature gradients very little experimental work has been done. Cunningham et al. (*7*) reported maximum temperature differences of 20°C. for the hydrogenation of ethylene on copper-magnesia catalyst pellets. Experimentally established effectiveness factors changed greatly with temperature. However the data were not compared with predictions based upon mass and heat transfer in the pellets. Miller and Deans (*8*) report temperature increases up to 33°C. No measurements of effectiveness factors were given.

In this work the reaction

$$2H_2 + O_2 \rightarrow 2H_2O \qquad (1)$$

$$\Delta H_{298°K.} = -115{,}600 \text{ cal./g.-mole}$$

was studied at 1 atm. pressure by using a 0.005 wt. % platinum on alumina catalyst. Because of the high ΔH and low k_e, temperature gradients are very high. However the activation energy is only 5,300 cal./g.-mole, so temperature variations do not have a large influence on the effectiveness factor. Particular care was taken to measure accurately the Δt between center and surface of the pellets. Values up to 300°C. were observed. Also the temperature changed significantly with position on the outer surface. For single pellets these results indicate that the usual assumption of radial heat flow may be but a rough approximation when the gas film resistance around the pellet varies greatly with peripheral position, as for example in a packed bed.

Experimental effectiveness factors were obtained directly by comparing rates of reaction for catalyst particles and for pellets. Sufficient kinetic data were measured to predict effectiveness factors from transport properties of the porous solid. Comparison of these results and intrapellet temperature differences were used to test the suitability of the transport properties and equations.

APPARATUS

The flow system used experimentally is represented schematically in Figure 1. Hydrogen and oxygen flows at constant pressure are provided from gas cylinders by using the constant head column (4). Hydrogen gas flows through the reference side of the conductivity cell (18) and through needle valves (3). The hydrogen and oxygen streams are mixed, the main part sent to the reactor (15) and the excess discharged to the atmosphere through a constant head column (8).

The gas mixture is cooled to —78°C. in dry ice trap (11) to eliminate condensable vapors, mainly water from the soap film meters (7, 10). The U tube (13) contains a mixture of silica gel and charcoal to remove possible poisons prior to the reactor. It was necessary to maintain this bed of particles at constant temperature to avoid perturbations in gas composition caused by adsorption and desorption of oxygen. The gas

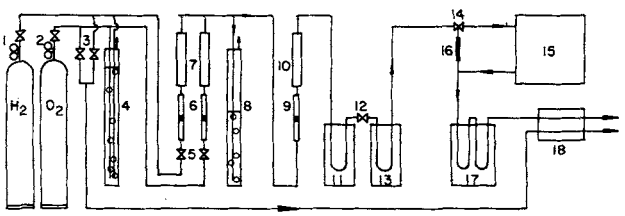

1, 2 H_2 and O_2 supply regulators
3, 5, 12 needle valves
14 three-way valve
6, 9 ball flowmeters
4, 8 constant head columns
11, 17 traps (-78°C)
13 silica gel-activated charcoal bed
15 reactor
16 capillary restriction
18 thermal-conductivity cell

Fig. 1. Flow diagram.

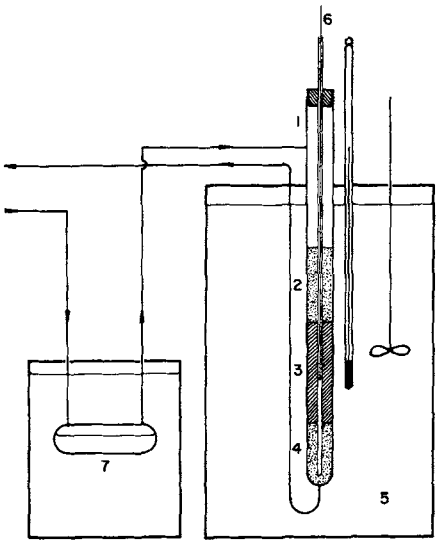

1 reactor
2, 4 glass beads (preheating and calming sections)
3 catalyst-diluent bed
5 constant temperature bath
6 moving thermocouple
7 saturator

Fig. 2. Reactor for catalyst particles.

leaving the reactor is cooled to —78°C. in the trap (17) and then flows through the sample side of the conductivity cell. The three-way valve (14) permits the feed gas to go to the reactor through the sample side of the cell. The apparatus was made primarily of Pyrex glass with Tygon tubing used for flexible connections and copper tubing for long lines. The equipment was shielded with a 5-mm. thick plate of Lucite to reduce danger in the event of explosions.

A tubular flow packed bed was used to measure the rate of reaction for the catalyst particles and a stirred-tank type of reactor was employed for the pellet measurements. These two reactors are shown in Figures 2 and 3.

Particle Reactor

To approach isothermal operation and obtain uniform velocity profiles, the 9.0-mm. I.D. reactor tube was packed with 25-mm. lengths of glass beads before and after the catalyst bed as indicated in Figure 2. The 0.005 wt. % platinum on alumina catalyst particles were diluted in a ratio of 1 to 10 with plain alumina particles. This mixture (0.1 to 0.4 g.) was further diluted with about 4.0 g. of glass beads (diameter = 85μ) to reduce the heat evolved per unit volume of bed. The length of the diluted bed was about 35 mm. The entire reactor was immersed in constant temperature bath (5).

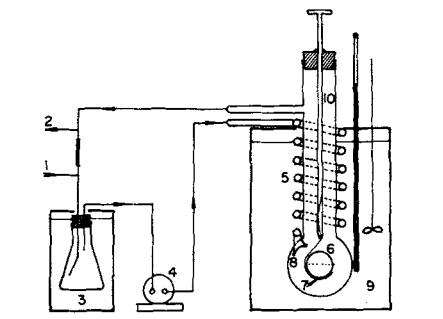

1 inlet
2 outlet
3 water trap (0 °C)
4 diaphragm pump
5 preheater
6 catalyst pellet
7 pellet support
8 entrance nozzles
9 constant temperature bath
10 glass rod

Fig. 3. Reactor for catalyst pellets.

Temperatures were measured with an iron-constantan thermocouple of 40 gauge (0.08-mm. diameter) wire inserted in a 0.7-mm. O.D. glass tube (6) running the length of the catalyst bed. The radial distribution of temperature in the bed was assumed to be parabolic, thus providing a method for obtaining the average temperature at any axial position from the measured temperatures at the center and at the wall (assumed equal to the bath temperature). Then the mean bed temperature was taken as the arithmetic average of the temperatures at four axial positions.

By maintaining a constant temperature at the saturator (7) a constant and known amount of water was added to the feed gas.

Pellet Reactor

The pellet reactor (Figure 3) was a spherical glass vessel of 44 mm. I.D. with a 21-mm. neck to permit passage of the 18.6-mm. catalyst pellets. The pellet (6) was supported with a fine stainless steel wire loop (7) which was held by glass rod (10).

To approach an ideal stirred-tank system, the reaction mixture was recycled through the neoprene diaphragm pump (4). The recycle and feed gases were preheated in the coil (5) and entered the reactor through the nozzles (8) to provide additional internal circulation. The recycle rate was constant at about 66 cc./sec. (STP), giving a recycle ratio from 13 to 42, by volume. The water trap (3), maintained at 0°C., held the water content of the reaction gases at a low and known value.

The thermal conductivity cell was calibrated by by-passing the reactor through the capillary (16) (Figure 1). The soap film meters (7) established the composition of this gas, which passed through the sample side of the cell. Periodic recalibration was needed. Differences between consecutive calibrations were only 1 to 2%, but the trend was in the same direction and became significant over a long time. The accuracy of the cell as an analytical device was tested by a gravimetric method which involved conversion of the oxygen to water by reaction, adsorption, and weighing of the water produced. The average deviation of the two methods of analysis was less than 5%.

As preliminary runs, the reactors without catalyst but with thermocouple wire, stainless steel wire (for pellet support), glass beads, and alumina were tested at severe reaction conditions. The catalytic activity thus observed was negligible.

CATALYST PREPARATION

A single batch of catalyst was prepared by wetting Boehmite (spray dried $Al_2O_3 \cdot H_2O$ from American Cyanamid Company) powder with a dilute solution of chloroplatinic acid. The resulting paste was dried at 80° to 90°C. for 24 hr., ground slightly to reduce particle agglomeration, and then heated in air at 550°C. for 5 hr. to decompose the chloroplatinic acid. At this stage the catalytic activity was poor and unstable.

Next, the catalyst was degassed in vacuum at 300°C. for 3 hr. and reduced in a stream of hydrogen at the same temperature for 5 hr. To reduce variations in activity in storage (due to exposure to air), a final treatment was given in which a stream of humid air at room temperature was passed through the particles for 8 hr.

A particle size range from 61 to 175μ (Tyler mesh No. 80-250) was selected for rate studies.

Pellets

The pellets, 1.86 cm. in diameter, were made by compressing mixtures of catalyst powder and alumina in hemispherical, stainless steel molds. To facilitate removal of the pellets, a very thin layer of stearic acid was deposited on the mold surface by first wetting it with a 1.0 wt. % solution in acetone followed by evaporation of the solvent. The amount of stearic acid introduced in a pellet in this way was not more than 0.5 mg. in comparison with a pellet weight of 2 g.

Pellets without thermocouples were pressed in one stage, while those with thermocouples required a two-stage process. Thermocouples were iron-constantan, Teflon-insulated, and 40 gauge to reduce the disturbance to the temperature field

Table 1. Characteristics of the Pellets

Pellet No.	Catalyst* dilution	Mass† of pellet, g.	Center and surface thermocouples	Pellet No.	Catalyst* dilution	Mass† of pellet, g.	Center and surface thermocouples
7	1/10	2.158	Yes	16	1/20	2.083	No
8	1/10	2.135	Yes	17	1/20	2.082	No
9	3/10	2.136	Yes	19	1/2.5	2.073	No
10	3/10	2.133	Yes	20	1/10	2.079	No
11	1/10	2.021	Yes	21	1/10	2.079	No
12	1/10	2.131	Yes	22	1/5	2.080	No
13	1/5	2.180	Surface only	23	1/2.5	2.078	No
				24	1/10	2.125	Yes
14	1/5	2.162	Yes	E	1/10	2.149	Yes

* Mass of catalyst powder/total mass of alumina plus catalyst powder.
† Mass is based upon weight of catalyst powder as taken from storage.

and to reduce conductivity error. A surface thermocouple was fixed in the lower hemisphere of the mold with at least a length of 0.5 cm. of wire running along the mold surface. The lower half of the pellet was then compressed and a second thermocouple placed with the bead at the center of flat surface. The pellet was completed by compressing the upper hemisphere in contact with the lower one. The position of the center thermocouple was verified by cutting some of the pellets. The bead size was about 0.2 mm. and the location of the surface couple was known within this distance. The position of the center couple was believed to be accurate to about ± 0.5 mm.

The pellets were prepared from mixtures of catalyst powder and inert homogeneous alumina. Dilution ratios from 1/2.5 to 1/20 were used in preparing pellets. Table 1 gives the conditions for each pellet used. Since the alumina and catalyst powder (99.995 wt. % alumina–0.005% platinum) have essentially the same properties, varying the dilution ratio provided a means of changing the Thiele modulus while maintaining constant physical properties of the pellets. This cannot be achieved, for example, by changing the temperature.

PROPERTIES OF CATALYST PELLETS

Since the catalyst powder and inert alumina are so similar, properties of the pellets may be measured by using mixtures of catalyst and alumina of any proportion, as long as the density is constant.

Thermal Conductivity

The effective thermal conductivity was measured on cylindrical pellets (5.0 cm. in diameter, 1.3 cm. in height) of the same density as the spherical pellets. The comparative method (6), with Lucite as the reference substance, was employed. This material has a conductivity of the same order as the pellet. The experimental value obtained with hydrogen in the pores and at 68.5°C. and 1 atm., was

$$k_e = 6.2 \times 10^{-4} \text{ cal./(cm.)(sec.)(°C.)} \qquad (2)$$

Table 2. Micro- and Macrovoid Fractions in Catalyst Pellets

Pellet No.	Micropore volume V_i, cc./g.	Macropore volume V_a, cc./g.	Solid volume V_s, cc./g.	Apparent pellet density ρ_p, g./cc.	Micropore void fraction ϵ_i	Macropore void fraction ϵ_a
8	0.400	0.987	0.373	0.568	0.227	0.561
14	0.400	0.933	0.373	0.586	0.234	0.547
16	0.400	0.997	0.373	0.564	0.226	0.563
23	0.400	0.997	0.373	0.564	0.226	0.563
Average:				0.57	0.228	0.558

Measurements on pellets of lower density were lower, as expected (6). The accuracy is believed to be about 10%. Since the pores will contain small amounts of oxygen and water vapor under reaction conditions, some modification of the result in Equation (2) will be necessary when calculating temperature gradients in reacting pellets.

Porosity Measurements

It is customary to divide the porosity of alumina pellets into two fractions: microporosity associated with pores for which $a < 100$ Å., and macroporosity in pores with radii > 100 Å. Because of the low density of the pellets used, the macropore contribution to transport properties is dominant; also the microporosity is not affected by the pelletting process.

The micropore properties of the same batch of alumina were measured by nitrogen adsorption by Otani (9) and are

$$V_i = 0.40 \text{ cc./g.}$$
$$\overline{a_i} = 27 \text{ Å.}$$
$$S_g = 300 \text{ sq. meters/g.}$$

The macropore volume distribution was measured in the range $a = 170$ to 90,000 Å. with an Aminco-Winslow mercury porosimeter. Four pellets of different dilutions, with and without thermocouples, but at the same density level were studied. The results for each pellet, as summarized in Table 2, are practically the same. The apparent density given in the fifth column was calculated as $1/(V_i + V_a + V_s)$. The solid volume V_s was based upon a true density for alumina of 2.68 g./cc., as reported by the alumina manufacturer. The average macropore radius, based upon volume, is 10,000 Å.

The macropore volume distribution as measured in the porosimeter for the pellets and for unconsolidated assembly of particles is shown in Figure 4. The micropore region gives the results obtained by Otani (9). The pellet curve shows the unusual behavior of two peaks in the macropore region, one at 5,500 Å. and a second at 30,000 Å. The first peak is due to macropores within the particles and second corresponds to void spaces between paticles. This can be seen by comparing porosity curves for the pellets with curves for unconsolidated particles, particles with no macropores, and with catalyst pellets of different densities.

The unconsolidated particle curve in Figure 4 shows a sharp maximum at about 6,500 Å. and another increase in porosity beginning at a radius of 15,000 Å. This second increase is a false one, corresponding to void spaces between particles. These spaces are caused by the agglomeration resulting from the pressure of the mercury. This was verified by measurements on unconsolidated particles of silica-alumina of the same size range. Again the increase in porosity at high a values was observed. even though there is no macropore porosity for this catalyst. The peak at 6,500 Å. agrees with the peak at 5,500 Å. on the pellet curve, thus identifying these macropores as void spaces within the particles.

Comparison of porosity curves at different pellet densities gives further evidence that the peak at 30,000 Å. corresponds

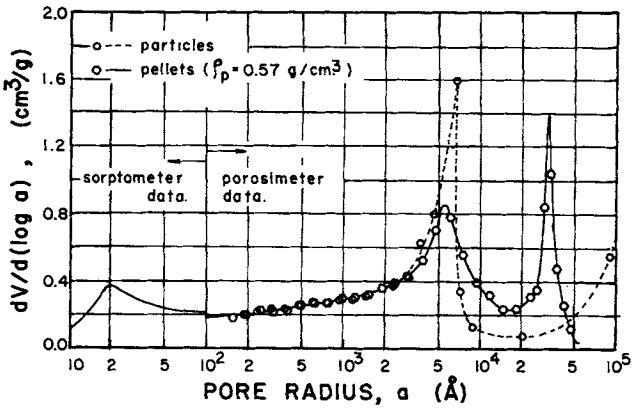

Fig. 4. Pore size distribution for particles and pellets ($\rho_p = 0.57$ g./cc.).

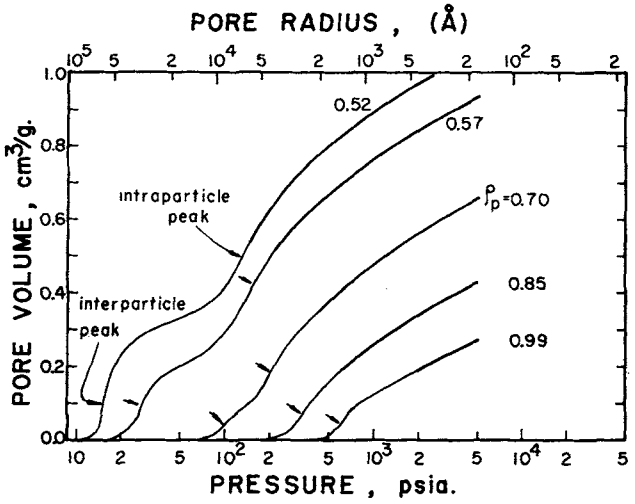

Fig. 5. Cumulative pore volume vs. pressure (porosimeter data).

to void spaces between particles. Figure 5 describes cumulative pore volume vs. pressure curves for densities from 0.52 to 0.99 g./cc. The arrows denote inflection points which locate the peaks on the distribution curves, such as Figure 4. The catalyst pellets used for rate studies have densities close to 0.57 g./cc. Increasing the density decreases both the size and volume of the interparticle pores. At $\rho_p = 0.7$ these pores have almost disappeared and at higher densities they do not exist. Since most alumina catalyst pellets have densities greater than 0.7, only one maximum in the macropore distribution curve is normally observed. The catalyst pellets used in the rate studies are unusual in this respect.

REACTION RATE RESULTS

Initially, feed compositions 0 to 4 mole % hydrogen were fed to the reactors. However the catalyst particles exhibited a 35-hr. period of nonsteady activity. The transient period for pellets was longer; the rate still decreased slowly after 50 hr. Further, water vapor affected the rate at temperatures up to 160°C. A few runs carried out at a partial pressure of water = 0.023 atm. with hydrogen pressures from 0.005 to 0.040 atm. indicated second-order kinetics with respect to hydrogen.

A more satisfactory behavior was found with feed gases in the other nonexplosive range, 0 to 6 mole % oxygen. Steady activity was reached after an initial 2-hr. period in which the rate increased with time. Water vapor had no measurable influence at temperatures above 80°C. Below 40°C. the reaction almost completely stopped. This was likely due to the strong adsorption or capillary condensation of water in the micropores. The reported data were obtained for the most part in this composition region, although a few measurements were made in the explosive range above 6 mole % oxygen. It was not possible to cool the apparatus and return to the same catalyst activity. Hence all runs with a given catalyst sample were completed before shutdown.

Particles

The average rate of reaction in the bed of catalyst particles was calculated from the differential reactor expression

$$\bar{r} = \frac{2F_{O_2}\, x}{m_c} \tag{3}$$

Because of the dilutions with inert alumina and glass beads the radial and axial temperature gradients were low. The mean bed temperature was never more than 2°C. above the bath temperature. Furthermore, for the rate equation obtained [Equation (4)] and the feed gas compositions, Equation (3) can be used with accuracy even for large conversions. For example, by using Equation (4) it can be shown that the error introduced in associating the rate from Equation (3) with the arithmetic average partial pressure of oxygen in the bed is less than 1% at a conversion of 25%. Hence differential reactor behavior could be assumed and rates could be evaluated from Equation (3) for all the observed data (average conversion = 25%). It should be noted also that the particle size is small enough to neglect heat and mass transfer resistances around and within the particles.

Rates were measured with twelve different samples of catalyst, since sample size was only about 0.02 g. Illustrative results are given in Table 3. The data covered the range:

$$\bar{p}_{O_2} = 0.0057 \text{ to } 0.0726 \text{ atm.}$$

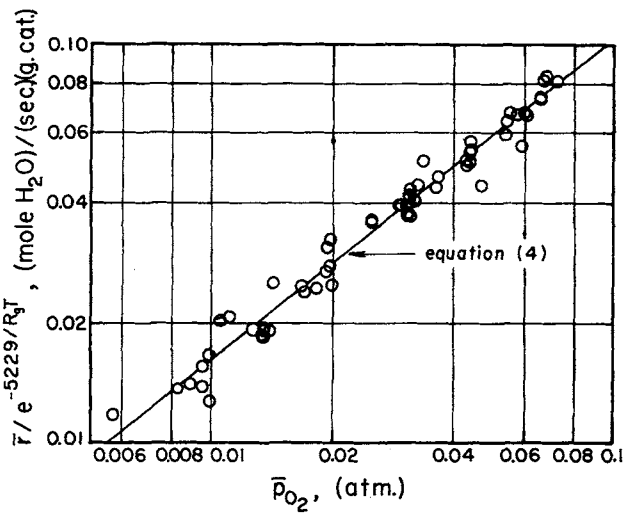

Fig. 6. Effect of oxygen partial pressure on reaction rate for catalyst particles.

Table 3. Illustrative Rate Data for Particles

Run No.	Mass of catalyst, g.	Bath temperature, °C.	Average bed temperature, °C.	$F \times 10^5$, mole/sec.	Oxygen partial pressure Inlet, atm.	Oxygen partial pressure Exit, atm.	Water partial pressure Inlet, atm.	Water partial pressure Exit, atm.	Hydrogen partial pressure Inlet, atm.	Hydrogen partial pressure Exit, atm.	Conversion x	$\bar{r} \times 10^6$, mole water / (sec.)(g.-cat.)
40	0.01843	141.5	141.8	5.82	0.0218	0.0146	0.0245	0.0375	0.982	0.948	0.316	43.3
43	0.01843	100.0	100.2	4.79	0.0218	0.0174	0.0261	0.0351	0.972	0.948	0.213	24.3
45	0.01801	141.4	142.0	4.84	0.0651	0.0437	0.0236	0.0654	0.939	0.891	0.324	112.8
47	0.01801	100.1	100.5	5.67	0.0653	0.0548	0.0232	0.0414	0.940	0.904	0.145	59.2
48	0.01801	80.5	80.7	2.81	0.0642	0.0538	0.0226	0.0434	0.925	0.903	0.162	32.9

Total pressure at inlet to reactor was a little higher than 1 atm. because of some pressure drop across the reactor.

$\bar{p}_{H_2O} = 0.0077$ to 0.0654 atm.

$\bar{p}_{H_2} = 0.891$ to 1.00 atm.

$\bar{t} = 60°$ to $200°C.$

All the data above 80°C. were correlated by the following equation:

$$r = 0.655\, p_{O_2}^{0.804} \exp\left(-\frac{5230}{R_g T}\right) \qquad (4)$$

with an average deviation of 6.6%. This expression was used to estimate rates at the pellet surface conditions in the calculation of experimental effectiveness factors and to compute the theoretical effectiveness factors.

The effect of $\bar{p}_{O_2}$ on the rate is shown in Figure 6 by the experimental points. The solid line represents Equation (4). Figure 7 shows the effect of temperature for various levels of oxygen partial pressure. Again the solid lines correspond to Equation (4). Deviations from the constant slope occur below 80°C. Note that the deviation is greatest for the runs with the highest $\bar{p}_{H_2O}$, suggesting that the effect may be due to competitive adsorption of water vapor. The activation energy of 5,230 cal./g.-mole agrees well with that found by Miller and Deans (8).

Pellets

The rate of reaction for the pellets could also be evaluated from Equation (3). However, the rate is not an average but a single value and the composition associated with the rate is that in the outlet stream. The rate is based upon the mass of undiluted catalyst in the pellet so that it will be on the same basis as the particle results.

Since the measurement of temperature differences was an important objective, it was vital to know if the observed ΔT were entirely due to the chemical reaction. Other temperature differences will be observed if the gases entering the reactor are not well mixed or preheated. A test run was made without oxygen in the feed. Thermocouples in three regions of the gas phase and the center and surface thermocouples in the pellet read within 0.3°C. of the bath temperature. In another test run the catalyst pellet was replaced with a pellet of pure alumina. No activity was observed.

The heat transfer resistance in the gas phase around the pellet was found to be significant, and its magnitude is discussed in the next section. It could be evaluated from the measured surface temperature. It is also desirable to know the mass transfer resistance, but surface concentrations were not measured. However, the concentration drop between bulk gas and solid surface could be estimated by two methods; both are based upon an analogy between mass and energy transfer. Thus for laminar flow, if the mechanism of transport and the effective gas film thickness are the same for mass and energy transfer

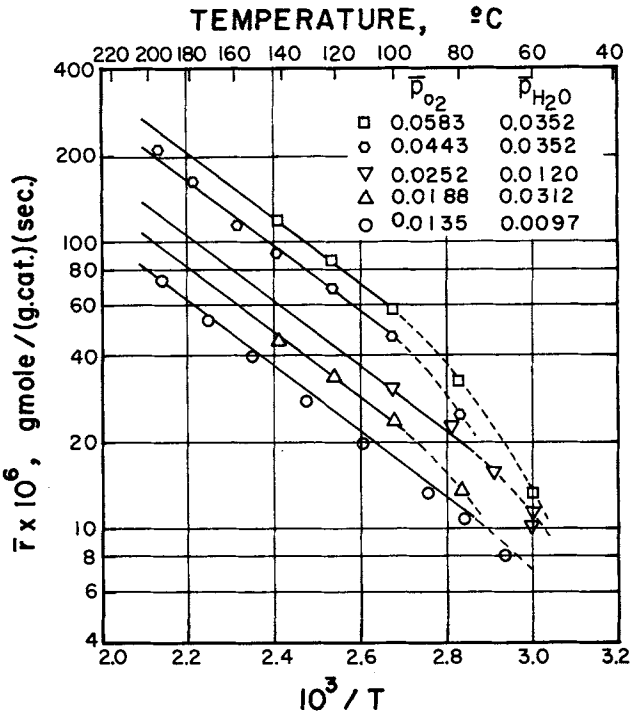

Fig. 7. Arrhenius plot for catalyst particles [solid line represents Equation (4)].

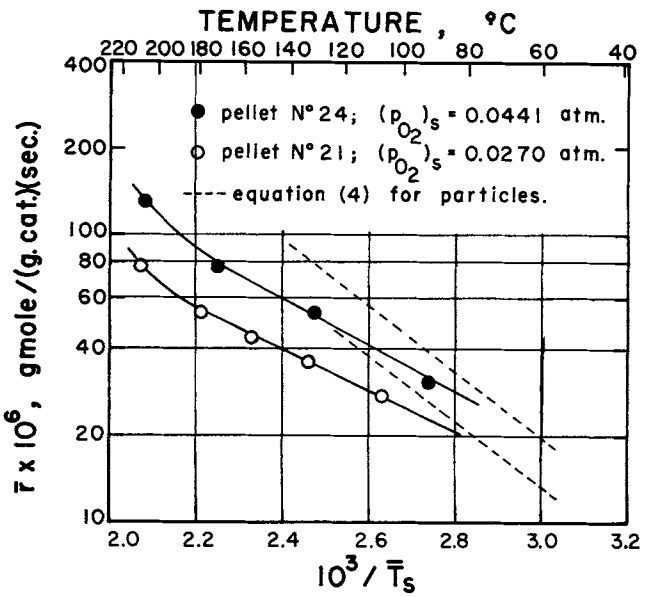

Fig. 8. Arrhenius plot for catalyst pellets.

TABLE 4. ILLUSTRATIVE DATA FOR CATALYST PELLETS

Pellet run*	Temperature measurements: Bath temperature, °C.	t_s,† °C.	t_c,† °C.	$F \times 10^5$, mole/sec.	Oxygen partial pressure: $(P_{O_2})_g$, atm.	$(P_{O_2})_s$, atm.	Ave. surface temp, $\bar{t}_s$, °C.	$\bar{r} \times 10^6$, moles water/(sec.)(g.-cat.)
11-1	95.0	100.7	124.1	11.6	0.0291	0.0283	101.3	28.5
11-2	89.9	100.8	147.7	8.57	0.0541	0.0527	101.0	49.8
11-3	97.5	99.5	107.2	10.5	0.0094	0.0091	99.6	9.5
12-3	90.3	101.5	150.1	11.7	0.0595	0.0579	101.9	49.8
24-1	180.6	205.8	254.6	14.6	0.0459	0.0423	207.7	125.6
24-3	119.1	130.3	171.6	14.3	0.0456	0.0441	131.0	51.8
E-1	83.6	117.6	219.2	20.4	0.111	0.107	116.7	140.5

* First number indicates the pellet number in Table 1.
† Average values of six rotation positions.

$$(C_g - C_s)_{O_2} = \frac{k_e (T_s - T_g)}{D_{O_2}(-\Delta H)} \qquad (5)$$

The temperature difference was measured and ΔH, the thermal conductivity of the gas k_g, and the diffusivity of oxygen are all known. The concentration change evaluated in this way was always less than 5% of $(C_{O_2})_s$. Since the flow is not completely laminar, Equation (5) is not exactly valid. As an alternate approach the Chilton-Colburn analogy was used to estimate the gas film concentration difference. In this case ΔC was somewhat less, not more than 4% of $(C_{O_2})_s$. While these analogies are not exact, particularly because of radiative heat transfer, the results show that the gas film mass transfer resistance cannot be large.* Hence surface concentrations evaluated from Equation (5) were used in calculating effectiveness factors in later sections.

Illustrative rate data for pellets are given in Table 4 along with oxygen partial pressures and total flow rates. The various temperatures, particularly the calculated average value, are discussed in the following section. Figure 8 is an Arrhenius plot of rate vs. calculated average surface temperature for two oxygen partial pressures. The dashed lines represent particle rates at the same oxygen concentration, as evaluated from Equation (4). The apparent activation energy for the pellets was about two-thirds of that for the particles. The points at the highest temperature, 200° to 220°C., seem to indicate a shift in activation energy, but measurements were not made at high enough temperatures for either particles or pellets to confirm this possibility. The results in Figure 8 indicate that the effectiveness factor for the pellet is less than unity down to the lowest temperatures studied. This is due primarily to the low activation energy.

INTRAPELLET AND GAS-PELLET TEMPERATURE DIFFERENCES

The pellet in the reactor was set on the glass rod support in such a way that the surface thermocouple was on the equator. By rotating the rod from outside the reactor it was possible to measure surface temperatures at any position on the equatorial line during a run. The results were as follows:

1. Pellet surface temperatures were 1° to 115°C. above the bath temperatures. Gas phase temperatures were between bath and surface values, thus indicating that gas film resistance to heat transfer was not negligible. Intrapellet temperature differences were much larger than those between pellet and gas. For run E-3, which was in the explosion range, $t_c - t_s$ was more than 300°C. Even for low reaction rates, run 14-3, the intraparticle Δt was about 9°C. It may be noted that the importance of the gas-to-pellet temperature difference with respect to intrapellet Δt depends upon the Thiele modulus Φ. In the region where the effectiveness factor decreases with Φ, the relative importances of the gas film Δt increases as Φ increases, since the heat of reaction is evolved closer to the pellet surface.

2. While the average reaction rate and the temperature at the pellet center were practically insensitive to rotation, the surface thermocouple readings were a strong function of position. Six readings of surface and center temperatures for successive rotations of about 30°C are given in Table 5 for low, intermediate, and high rates. The differences around the surface increased with rate and were largest for run E-3 where a maximum Δt_s of 97°C. was observed.

* Hutchings and Carberry (*10*) also predict that negligible mass transfer and finite heat transfer resistances are expected under some conditions.

Table 5. Surface Temperature Measurements on Equator of Pellets

Run No.	Bath temp., °C.	Temperature readings by rotation of pellet: Surface, °C.	Center, °C.	Reaction rate per pellet $r_p = mc\bar{r}$, mole/(sec.)(pellet)
		103.3	158.2	
		99.7	158.2	
14-2	81.7	104.2	158.3	21.0×10^{-6}
		114.5	158.4	
		94.9	158.6	
		107.5	158.6	
		96.3	105.7	
		95.6	105.7	
		95.6	105.7	
14-3	92.4	97.3	105.7	3.5×10^{-6}
		95.4	105.7	
		96.3	105.9	
		151.9	474.2	
		157.0	476.6	
E-3	65.0	187.8	478.6	
		166.4	486.1	
		169.5	477.3	88.0×10^{-6}*
		248.8	488.4	

* Not measured; estimated value from $(t_c - \bar{t}_s)$ data.

Since rotation does not change the thermocouple locations with respect to the pellet, the differences in t_s must be due to local variations in heat transfer coefficient h_g between gas and pellet. These variations, due to unsymmetrical mixing, indicate that the radial heat flow model is an approximation. The approximation may be reasonably valid provided the variations in surface temperature are moderate and average values for T_s and h_g are used.

In order to be able to assume radial heat flow for effectiveness factor calculations, an average t_s was computed in the following way. First, surface temperatures were measured for three pellets in fourteen locations (six positions equally spaced on the equator and four locations in each hemisphere). Then local values of h_g were estimated for each location by using the equation

$$h_g = \frac{Q_p}{A_p(t_s - t_w)} = \frac{(-\Delta H)\, r_p}{A_p(t_s - t_w)} \qquad (6)$$

This expression supposes that the local heat flux is equal to the average value Q_p/A_p. This will be a good approximation if the variations in t_s are small enough that radial heat flow is valid. Thus Equation (6) should give reliable results for runs such as 14-2 and 14-3 but probably not for run E-3 (see Table 5). For applicable cases the local coefficient varies twofold, with an arithmetic average of 0.99×10^{-2} cal./(sq.cm.)(sec.)(°C.). Since the pellet location and recirculation rate in the reactor were the same for all the runs, $\bar{h}_g$ should be approximately constant. Finally, this average value of h_g was used in Equation (6) to calculate an *average* t_s for all the pellet data. It is this temperature that is given in the next to last column of Table 4.

EFFECTIVENESS FACTORS

Experimental Values

$(E.F.)_{exp}$ is the measured rate of reaction for the pellet divided by the rate at surface conditions. The latter can be evaluated from Equation (4) at surface conditions if it is assumed that the catalytic activity of a particle in the pellet is the same as the activity of the particle by itself.

Table 6. Computed and Experimental Effectiveness Factors

Run No.	Φ_s	β	γ	E.F. Predicted	E.F. Exp.	$T_c - T_s$ exp., °C.
7-1	2.67	0.030	7.00	0.78	0.67	8.4
8-3	2.47	0.085	6.90	0.87	0.87	26.4
8-4	2.44	0.131	6.81	0.94	0.93	41.5
8-7	2.00	0.136	7.27	1.01	0.96	36.9
11-2	2.17	0.116	7.03	0.95	0.92	46.7
E-1	2.17	0.339	6.75	1.42	1.10	102.5
14-2	3.14	0.161	6.96	0.89	0.80	53.6
10-2	4.53	0.116	6.58	0.64	0.60	41.9
10-6	3.04	0.144	7.52	0.89	0.79	47.2

At high pellet densities crushing of the particles during pelletization might change the activity, but for the low density pellet used here this is unlikely. Hence

$$(\text{E.F.})_{\text{exp}} = \frac{\bar{r}}{r_s} = \frac{\bar{r}}{0.655 (P_{O_2})_s^{0.804} \exp\left[-\dfrac{5230}{R_g \bar{T}_s}\right]} \tag{7}$$

where $\bar{T}_s$ is the average surface temperature. $(\text{E.F.})_{\text{exp}}$ from Equation (7) are given in Table 6.

Prediction Method

Assuming again that the particle rate is the same in the pellet as measured for beds of unconsolidated particles, one can use mass and energy balance equations to predict an effectiveness factor. Additional assumptions are: constant k_e and D_e within the pellet, mass and heat transfer by bulk flow and heat transfer by radiation within the pellet are negligible, and radial heat and mass transfer and constant surface temperature and concentration.

In terms of the oxygen gradient, $(\text{E.F.})_{\text{pr}}$ is given by

$$(\text{E.F.})_{\text{pr}} = \frac{2 A_p D_e \left(\dfrac{dC_{O_2}}{dR}\right)_{R_o}}{m_p (\text{D.R.})\, r_s} = \frac{6 D_e \left(\dfrac{dC_{O_2}}{dR}\right)_{R_o}}{R_o \rho_A r_s} \tag{8}$$

where the factor of 2 is needed because the rate is expressed as water produced while the gradient is expressed in oxygen concentration. In terms of the Thiele modulus Φ_s and dimensionless variables, Equation (8) is

$$(\text{E.F.})_{\text{pr}} = \frac{3}{\Phi_s^2} \left(\frac{dy}{d\xi}\right)_{\xi=1} \tag{9}$$

$$\Phi_s = R_o \left(\frac{r_s \rho A}{2 D_e (C_{O_2})_s}\right)^{1/2} \tag{10}$$

$$y = \frac{C_{O_2}}{(C_{O_2})_s} \tag{11}$$

$$\xi = \frac{R}{R_o} \tag{12}$$

To obtain $\left(\dfrac{dy}{d\xi}\right)_{\xi=1}$, the following differential mass balance within the pellet must be solved:

$$\frac{d^2y}{d\xi^2} + \frac{2dy}{\xi d\xi} - \Phi_s^2 \left(\frac{r}{r_s}\right) = 0 \tag{13}$$

The ratio r/r_s is necessary because Φ_s applies to conditions at the pellet surface. From Equation (4)

$$\left(\frac{r}{r_s}\right) = \frac{0.655 (p_{O_2})^{0.804} \exp\left(\dfrac{-5230}{R_g T}\right)}{0.655 (p_{O_2})_s^{0.804} \exp\left(\dfrac{-5230}{R_g T_s}\right)} \tag{14}$$

or in dimensionless parameters

$$\frac{r}{r_s} = \left(y \frac{T}{T_s}\right)^{0.804} \exp\left[\gamma \left(1 - \frac{T_s}{T}\right)\right] \tag{15}$$

The Damkoehler relationship between concentration and temperature can be used instead of writing a differential energy balance; this is

$$T - T_s = (-\Delta H) \frac{D_e}{k_e} [(C_{O_2})_s - C_{O_2}] \tag{16}$$

or in dimensionless form

$$\frac{T}{T_s} = 1 + \beta - \beta y \tag{17}$$

$$\beta = \frac{(-\Delta H) D_e (C_{O_2})_s}{k_e T_s} \tag{18}$$

Combination of Equations (16), (18), and (15) and substitution of the resultant expression for r/r_s in Equation (13) give the following equation for y as a function of ξ:

$$\frac{d^2y}{d\xi^2} + \frac{2}{\xi}\frac{dy}{d\xi} - \Phi_s^2 [(1 + \beta - \beta y) y]^{0.804} \exp\left[\gamma \left(\frac{\beta - \beta y}{1 + \beta - \beta y}\right)\right] = 0 \tag{19}$$

with boundary conditions

$$\left.\begin{aligned} y &= 1 \text{ at } \xi = 1 \\ \frac{dy}{d\xi} &= 0 \text{ at } \xi = 0 \end{aligned}\right\} \tag{20}$$

Equations (19) and (20) were solved numerically and $(\text{E.F.})_{\text{pr}}$ was evaluated from Equation (9) by machine computation for a range of values of γ (from 5 to 15) and β which covered the experimental hydrogen-oxygen system. The integration was carried out from surface to center of the pellet by using 50 to 300 radial increments.

For the initial value of $\left(\dfrac{dy}{d\xi}\right)_{\xi=1}$ needed to start the computations, the well-known result for the first-order iso-

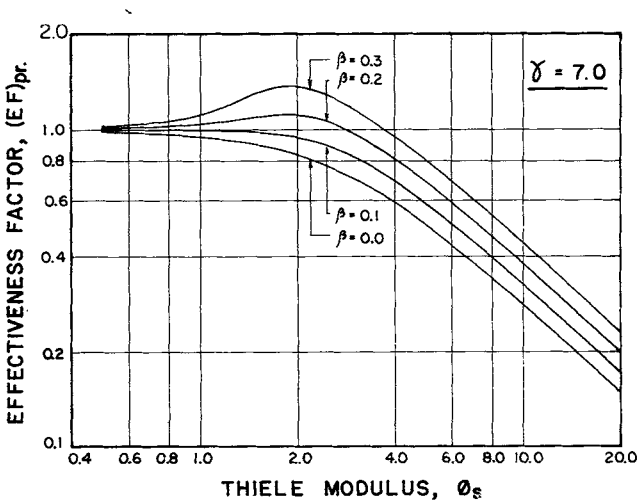

Fig. 9. Computed effectiveness factors.

thermal problem was used. This gave a lower limit to $(E.F.)_{pr}$, since for both kinetics of less than first order and an exothermic reaction, E.F. will increase. The computer results were checked with the analytical solution for first-order isothermal conditions to establish the size of increment required for 0.1% precision. Most of the experimental data were for values of γ near 7.0 (see Table 6). In Figure 9 the computed results are illustrated by plotting $(E.F.)_{pr}$ vs. β and Φ_s for this level of γ. The effect of nonisothermal conditions is evident by comparison of the curves with that for $\beta = 0$.

Effective Thermal Conductivity and Diffusivity

To predict E.F. from the computed results, k_e and D_e are required. The effective thermal conductivity under reaction conditions can be obtained by making corrections, for temperature and composition changes, to the measured value [Equation (2)]. The effective diffusivity can be estimated from the random pore model (*11*) by using the porosity and pore volume distribution data in Table 2 and Figure 4. However the very low density of the catalyst and the resulting three peaks in Figure 4, rather than the usual two, create uncertainties in applying the model. If the very large pores (peak at 30,000Å.), which disappear for pellets of higher density, are neglected $(D_e)_{100°C.}$ is found to be 0.15 sq.cm./sec. The other extreme in diffusivity would result if the micropores in the model are restricted to those of radius less than 100Å. and the two peaks at larger radii are assumed to be macropores. Under these conditions $(D_e)_{100°C.} = 0.32$ sq.cm./sec. Both calculations are based upon estimating a bulk diffusivity for oxygen in the gas mixture at 100°C. For an average gas composition in the pellet of 95.1 mole % hydrogen, 1.6% oxygen, and 3.3% water, this value is $(D_{O_2})_{100°C.} = 1.05$ sq.cm./sec.

Fortunately, another method of obtaining D_e can be derived in terms of the temperature measurements. This approach has the added advantage of giving D_e directly at reaction conditions. It is based upon Equation (16) applied at the center of the pellet; that is

$$\left(\frac{D_e}{k_e}\right) = \frac{T_c - \overline{T}_s}{(-\Delta H)\,[(C_{O_2})_s - (C_{O_2})_c]} \qquad (21)$$

As the diffusional resistance increases, $(C_{O_2})_c$ approaches zero. Hence, the limiting form of Equation (21) establishes D_e/k_e as

$$\left(\frac{D_e}{k_e}\right) = \lim_{\Phi_s\sqrt{D_e}\to\infty}\left[\frac{T_c - \overline{T}_s}{(-\Delta H)\,(C_{O_2})_s}\right] \qquad (22)$$

All the quantities in brackets are measured and k_e was determined separately. Hence D_e can be estimated from the limit of a plot of the term in brackets vs. $\Phi_s\sqrt{D_e}$. The quantity $\Phi_s\sqrt{D_e}$ measures the diffusion resistance equally well as Φ_s but has the advantage that D_e is not needed for its evaluation.

Both D_e and k_e vary slightly with temperature so that Equation (22) defines a ratio at some average temperature which varied from run to run. To account for this effect, both sides of Equation (22) were multiplied by a correction factor f to give

$$\left(\frac{D_e}{k_e}\right)_{100°C.} = \lim_{\Phi_s\sqrt{D_e}\to\infty}\left[\frac{f(T_c - \overline{T}_s)}{(-\Delta H)\,(C_{O_2})_s}\right] \qquad (23)$$

and

$$f = \frac{(D_e/k_e)_{100°C.}}{(D_e/k_e)_{\overline{T}_p}} \qquad (24)$$

The factor f was estimated by taking into account the effects of temperature on k_{O_2} and D_{O_2}. Figure 10, a plot

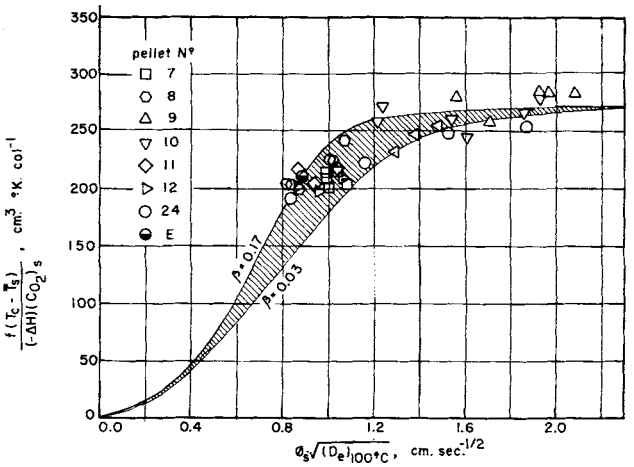

Fig. 10. Estimation of (D_e/k_e).

of the data according to Equation (23), does indicate that a limit is approached and that its value is

$$\left(\frac{D_e}{k_e}\right)_{100°C.} = 272 \text{ cc./(°K.)(cal.)} \qquad (25)$$

The measured k_e [Equation (2)] was for hydrogen filling the pores and at 68.5°C. A small correction should be applied to this value before using it in Equation (25). By taking the average composition of the gas in the pellet given earlier, calculations suggest that these two effects just about balance, giving k_e for pellet conditions at 100°C. as 6.1×10^{-4} cal./(cm.)(sec.)(°C.). By using this result in Equation (25), the diffusivity under reaction conditions is

$$(D_e)_{100°C.} = 0.166 \text{ sq.cm./sec.} \qquad (26)$$

This result, which is close to the lower extreme calculated from the random pore model, is probably the most reliable and is used in later calculations of $(E.F.)_{pr}$. In view of the thousandfold range of diffusivities reported in the literature for porous catalysts, the similarity in the results found by the two methods is encouraging.

It should be noted that Equation (23) is independent of the kinetic measurements; therefore $(E.F.)_{exp}$ was not used in obtaining D_e.

Predicted E.F.

With k_e, D_e, and $\overline{T}_s$ known, β, Φ_s, and γ can be evaluated for each pellet run and used with charts like Figure 9 to determine $(E.F.)_{pr}$. Average values of k_e and D_e, corresponding to $\overline{T}_p$, were used to calculate β and Φ_s. A few of the results are given in Table 6. Agreement of experimental and predicted results is reasonably good (about 7% average deviation) except for pellets No. 21, 24, and E. There is reason to believe that the catalyst was deactivated in pellets No. 21 and 24 by poisoning vapors from the Tygon connections in the recycle line. Data for run E were taken in the explosion range where particle kinetic data had to be obtained by extrapolation and the gases contained considerable water, thus reducing the effective diffusivity.

The predicted results are consistently higher than $(E.F.)_{exp}$ as seen in Figure 11. Several reasons could explain the deviation: a decrease in activity of the catalyst particles of about 7% during the pellet process, caused perhaps by blocking of some of the smaller pores; estimated D_e is high; and estimated $\overline{T}_s$ is high because of errors in temperature measurements. The first explanation seems the more probable. Both the second and third pos-

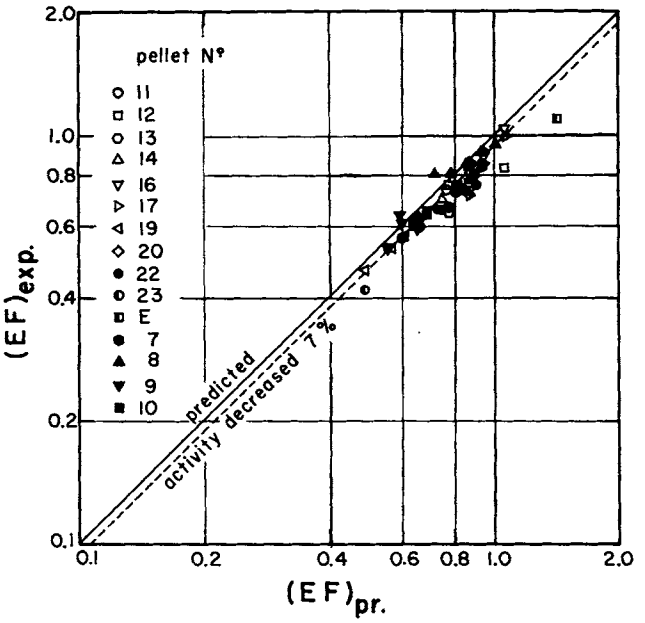

Fig. 11. Experimental vs. computed effectiveness factors.

sibilities would lead to differences between predicted and experimental E.F. that were high at large values of Φ_s (low E.F.) and small at low Φ_s. However Figure 11 shows that the deviation is essentially constant. The dotted line corresponding to a decrease in catalyst activity of 7% fits the data with about the same precision as Equation (4) correlates the particle rates.

PREDICTED TEMPERATURE DIFFERENCES

Equation (21) can be used to predict $T_c - \overline{T}_s$ by using Equation (25) for D_e/k_e. The agreement of the temperature difference so evaluated with the measured result is given by the consistency of the points in Figure 10. The points should not fall on a single curve, since β varies from run to run. The shaded area corresponds to β from 0.03 to 0.17 which include β values for most of the runs. The data fit the shaded region quite well. This test is significant because the functions plotted include experimental errors in composition and temperature measurements, reproduction of pellets, and estimation of the average heat transfer coefficient.

CONCLUSIONS

1. The possibility of very high temperature differences between the center and surface of catalyst pellets has been confirmed experimentally. It is important to note that the temperature difference for given Φ_s, β, and γ is independent of pellet size. Large pellets were used in this study to simplify and increase the accuracy of the experimental methods.

2. Large variations in surface temperature with position were observed at high reaction rates. This variation should be more pronounced in beds of pellets than for the single pellet case studied here. Despite these variations, the radial heat flow model gave a satisfactory prediction for E.F. if an average surface temperature, defined with Equation (6), were used.

3. The predicted and experimental E.F. and $(T_c - \overline{T}_s)$ agreed well, but it is probable that a small (7%) decrease in catalytic activity occurred during the pellet process.

4. A method of evaluating D_e at reaction conditions was proposed which relates the effective diffusivity to the thermal conductivity and $T_c - \overline{T}_s$ through the Damkoehler equation.

Finally, it may be noted that Φ_s should be in the range 0.6 to 5.0 in order to measure accurately large intrapellet temperature differences. If Φ_s is much less than 0.6 the temperature rise will be small. If $\Phi_s > 5.0$, the temperature rise will be close to the maximum, but will exist as a very sharp increase near the pellet surface. For example, for $\Phi_s = 10$, $\gamma = 7.0$, and $\beta = 0.2$, nearly 99% of the rise will be between R/R_o of 0.8 and 1.0. This makes it extremely difficult to measure the surface temperature accurately.

ACKNOWLEDGMENT

The financial assistance of the National Science Foundation through Grant No. GP 2990, the Fellowship Award of the Consejo Nacional de Investigaciones Científicas y Técnicas, Argentina, to J. A. Maymo, and the support of the Computer Center at Davis through National Institutes of Health Grant No. FR-00009, are all gratefully acknowledged. The discussions with Professor P. L. Silveston on parts of the work were most helpful.

NOTATION

a = pore radius, Å.
A_p = external area of catalyst pellet, sq. cm.
C = concentration, g.-mole/cc.
D = bulk diffusivity, sq. cm./sec.
$D.R.$ = dilution ratio, (g.-catalyst at storage conditions)/(g.-catalyst + g. alumina)
D_e = effective diffusivity of oxygen in pellets, sq. cm./sec.
E = activation energy, cal./g.-mole
f = temperature correction factor, defined by Equation (24)
E.F. = effectiveness factor of pellet
F = total feed rate, F_{O_2} = oxygen feed rate, g.-mole/sec.
ΔH = heat of reaction, cal./g.-mole
h_g = gas-to-pellet heat transfer coefficient, cal./(sq. cm.)(sec.)(°C.)
k_e = effective thermal conductivity of pellet, cal./(cm.)(sec.)(°C.)
k_g = thermal conductivity of gas, cal./(cm.)(sec.)(°C.)
m_c = mass of undiluted catalyst, g.
m_p = mass of pellet, g.
p = partial pressure, atm.
Q_p = rate of heat evolution per pellet, cal./sec.
R = radial distance in spherical pellet; R_o = radius, cm.
R_g = gas constant, cal./(g.-mole) (°K.)
r = rate of reaction, moles water produced/(g. of undiluted catalyst at storage conditions)(sec.)
$\bar{r}$ = average rate, for pellet or for bed of particles
r_s = rate at pellet surface conditions
S_g = pore surface area, sq. meter/g.
T = temperature, $\overline{T}_p$ = mean temperature of pellet, °K.
t = temperature, °C.
V = pore volume
x = conversion of oxygen
y = $(C_{O_2})/(C_{O_2})_s$

Greek Letters

γ = E/R_gT_s
β = defined by Equation (18)
ϵ = void fraction
ρ_p = density of catalyst pellet, g./cc.
ρ_A = mass of undiluted catalyst (at storage conditions) per unit volume of pellet, g./cc.

Φ_s = Thiele modulus, defined by Equation (10)
ξ = R/R_o

Subscripts and Superscripts

— = average value
b = average bed condition (for particles)
c = catalyst or center
a,i = macro- and micropores, respectively
exp = experimental
g = bulk gas phase
p = pellet
s = solid or outer surface of pellet
pr = predicted
w = reactor wall condition

LITERATURE CITED

1. Carberry, J. J., *A.I.Ch.E. J.*, 7, 350 (1961).
2. Tinkler, J. D., and A. B. Metzner, *Ind. Eng. Chem.*, 53, 663 (1961)
3. Weisz, P. B., and J. S. Hicks, *Chem. Eng. Sci.*, 17, 265 (1962).
4. Satterfield, C. N., and T. K. Sherwood, "The Role of Diffusion in Catalysis," Chap. 3, Addison-Wesley, Reading, Mass. (1963).
5. Sehr, R. A., *Chem. Eng. Sci.*, 9, 145 (1958).
6. Masamune, Shinobu, and J. M. Smith, *J. Chem. Eng. Data*, 8, 55 (1963).
7. Cunningham, R. E., J. J. Carberry, and J. M. Smith, *A.I.Ch.E. J.*, 11, 636 (1965).
8. Miller, D. N., and H. A. Deans, paper presented A.I.Ch.E. San Francisco meeting (May, 1965).
9. Otani, Seiya, Noriaki Wakao, and J. M. Smith, *A.I.Ch.E. J.*, 11, 439 (1965).
10. Hutchings, John, and J. J. Carberry, *ibid.*, 12, 20 (1966).
11. Wakao, Noriaki, and J. M. Smith, *Chem. Eng. Sci.*, 17, 825 (1962).

Manuscript received December 6, 1965; revision received March 4, 1966; paper accepted March 7, 1966.

Shape of Liquid Drops Moving in Liquid Media

R. M. WELLEK, A. K. AGRAWAL

University of Missouri, Rolla, Missouri

and A. H. P. SKELLAND

University of Notre Dame, Notre Dame, Indiana

An investigation of the effects of various physical properties, drop size, and drop velocity on drop shape was carried out for nonoscillating liquid drops falling through stationary liquid continuous phases. The data of forty-five dispersed-continuous phase systems were studied with continuous phase viscosities varying from 0.3 to 46 centipoise and interfacial tensions varying from 0.3 to 42 dyne/cm. A theoretical relation was obtained from the Taylor and Acrivos analysis which quite accurately predicts drop eccentricities for drop Reynolds numbers less than about 20, but is highly inaccurate at higher Reynolds numbers. Relatively simple empirical relations involving the Weber number, Eötvös number, and viscosity ratio were obtained which enable the prediction of the eccentricity of nonoscillating drops over a wide range of Reynolds numbers (6.0 to 1,354) with average deviations of 6 to 8%. These relations may be useful in the estimation of the interfacial area, velocity, and continuous phase mass transfer coefficient of drops distorted from spherical shape.

In liquid-liquid extraction, mass transfer between phases is often facilitated by dispersing one phase in the other. Many investigators have studied mass transfer from single liquid droplets in order to obtain information which might ultimately aid in the design of large-scale extraction columns without the need for experimentally measured overall extractor efficiencies (*11, 18, 23, 26, 33, 36, 38*). Most of these studies have been based on the assumption of spherical droplets. At low droplet Reynolds numbers, droplet shape will approximate a sphere; however, at high Reynolds numbers droplets will be distorted from spherical shape. The change in shape affects not only interfacial area but also, as indicated by recent experimental and theoretical studies (*2, 24, 32*), the continuous phase mass transfer coefficient. While several investigators (*4, 6, 10, 14, 19, 22*) have reported quantitative information on the shape of liquid droplets for individual systems, currently there is no accurate means of predicting droplet shape without recourse to experiment.

It is the purpose of the present investigation to obtain a relation which will predict the shape of nonoscillating liquid droplets moving in liquid media from a knowledge of the physical properties of the Newtonian dispersed and continuous liquid phases, the droplet size, and relative droplet velocity.

PREVIOUS WORK AND THEORETICAL CONSIDERATIONS

Droplet Shape

The shape of a drop moving in a liquid continuous phase is determined by the forces acting along the surface of the drop. Basically the shape is dependent upon